Published in final edited form as:
Phys Med Biol. 2010 September 21; 55(18): 5417–5435. doi:10.1088/0031-9155/55/18/010.

Modeling the Detectability of Vesicoureteral Reflux using Microwave Radiometry

Kavitha Arunachalam[1,*], **Paolo F. Maccarini**[2], **Valeria De Luca**[3], **Fernando Bardati**[4], **Brent W. Snow**[5], and **Paul R Stauffer**[2]

[1] Dept of Engineering Design, Indian Institute of Technology Madras, India

[2] Dept of Radiation Oncology, Duke University Medical Center, Durham USA

[3] Dept of Information Tech & Electrical Eng., ETH Zurich

[4] Dept of Computer Science, Systems & Production, University of Rome, Tor Vergata

[5] University of Utah and Primary Children's Medical Center, Salt Lake City USA

Abstract

We present the modeling efforts on antenna design, frequency selection and receiver sensitivity estimation to detect vesicoureteral reflux (VUR) using microwave (MW) radiometry as the warm urine from the bladder maintained at fever range temperature using a MW hyperthermia device reflows into the kidneys. Radiometer center frequency (f_c), frequency band (Δf), and aperture radius (r_a) of the physical antenna for kidney temperature monitoring are determined using a simplified universal antenna model with circular aperture. Anatomical information extracted from computed tomography (CT) images of children age 4–6 years is used to construct a layered 3D tissue model. Radiometric antenna efficiency is evaluated in terms of the ratio between the power collected from the target at depth and the total power received by the antenna (η). Power ratio of the theoretical antenna is used to design a microstrip log spiral antenna with directional radiation pattern over $f_c \pm \Delta f/2$. Power received by the log spiral from the deep target is enhanced using a thin low-loss dielectric matching layer. A cylindrical metal cup is proposed to shield the antenna from electromagnetic interference (EMI). Transient thermal simulations are carried out to determine the minimum detectable change in antenna brightness temperature (δT_B) for 15–25 mL urine refluxes at 40–42°C located 35 mm from the skin surface. Theoretical antenna simulations indicate maximum η over 1.1–1.6 GHz for r_a = 30–40 mm. Simulations of the 35 mm radius tapered log spiral yielded higher power ratio over $f_c \pm \Delta f/2$ for the 35–40 mm deep targets in the presence of an optimal matching layer. Radiometric temperature calculations indicate $\delta T_B \geq 0.1$ K for the 15 mL urine at 40°C and 35 mm depth. Higher η and δT_B were observed for the antenna and matching layer inside the metal cup. Reflection measurements of the log spiral in saline phantom are in agreement with the simulation data. Numerical study suggests a radiometer with f_c =1.35 GHz, Δf = 500 MHz and detector sensitivity better than 0.1 K would be the appropriate tool to noninvasively detect VUR using the log spiral antenna.

Keywords

microwave radiometry; antenna design; vesicoureteral reflux; urinary tract infection; noninvasive thermometry; thermal noise

[*]Corresponding author: Kavitha Arunachalam, akavitha@iitm.ac.in.

1. Introduction

Vesicoureteral reflux (VUR) is an abnormality in the urinary system that causes urine inside the bladder to flow backwards to the kidney. VUR predisposes children with urinary tract infection (UTI) to bacterial infection and renal scaring potentially leading to kidney damage [1,2]. The severity of reflux is designated into grades I–V and the rate of renal scarring is high in children with high grade VUR [3]. The incidence of VUR in children with UTI is about 30% [3,4]. Children and infants with swollen kidney prior birth undergo voiding cystouretherography (VCUG) or radionuclide cystography (RNC) diagnostic tests [5]. The imaging studies involve bladder catheterization, ionizing radiation and reflux of urine from bladder to kidneys is monitored using X-ray or scintillation images. The risks of long term effects from exposure to ionizing radiation [6–8] and unpleasant bladder catheterization provide the motivation to develop non-invasive and non-ionizing techniques to detect VUR [9–11]. In [11], a passive MW diagnostic system is introduced to detect the reflux using a radiometer as the warm urine from the noninvasively heated bladder reflows into the kidneys 3–5°C above the surrounding tissue temperature. In the proposed system, urine inside the bladder is raised to fever range temperature of 40–45°C using an external 915 MHz MW hyperthermia device requiring no catheterization or radiation exposure. In this work we present the theory and modeling efforts for the radiometric antenna design, frequency selection and detector sensitivity estimation for the system used in the animal study [11].

MW radiometry has been used in medicine for noninvasive thermal monitoring of biological tissues several centimeters deep [12,13]. Application of MW radiometry in medicine include breast cancer detection [14,15], brain temperature monitoring in newborn infants [16–18], ablation and hyperthermia temperature monitoring [19–22], cerebral temperature monitoring and brain functional imaging [23,24]. A typical MW radiometer gathers thermal radiation from biological tissues using an antenna in the lower spectrum of the microwaves (1–5 GHz). Extremely low energy expressed as power spectral density on the order of 10^{-20} Watts/Hz (or Joule) received by the antenna is amplified and processed by low loss and low noise MW components to retrieve tissue temperature information [19,25]. The brightness temperature measured by the radiometer over the i^{th} frequency band using an antenna located at position $\vec{r}$, is the sum of the weighted volume average of the tissue temperature $T(\vec{r}', t)$, in the antenna sensing volume V, the EMI collected by the antenna from the surrounding T_{EMI}, the noise temperature of the radiometer system components T_{sys}, and is given by [25],

$$T_{B,i}(\vec{r},t)=\int_B \gamma df \int_V W(\vec{r},\vec{r}',f)T(\vec{r}',t)dv+T_{EMI}+T_{sys}; \quad r \notin V. \tag{1}$$

In Eqn (1), W is the radiometric weighting function given by,

$$W(\vec{r},\vec{r}',f)=\frac{P_d(\vec{r},\vec{r}',f)}{\int_V P_d(\vec{r},\vec{r}',f)dv} \tag{2}$$

with $\int_V W(\vec{r},\vec{r}',f)d\vec{r}'=1$, γ is the antenna power transmission coefficient and B is the radiometer bandwidth. In Eqn (2), $P_d = \sigma/2|\vec{E}(\vec{r}, \vec{r}', f)|^2$ is the power density deposited by the radiometric antenna inside V which is same as the received power density from reciprocity

theorem; σ and $\vec{E}$ are the tissue electrical conductivity and electric field vector inside antenna sensing volume (V) respectively. The design of a MW radiometer involves building a receiver with low noise MW components and shielding from external EMI to reduce T_{sys} and T_{EMI} respectively. Another key aspect is the design of the receive antenna with directional radiation pattern and higher power transmission (η, γ respectively) for enhanced contribution from the target at depth. The last component is the inversion algorithm for retrieving absolute tissue temperature at depth from the brightness temperature measurements.

In this work we focus on the receive antenna design and evaluate the radiometer receiver sensitivity required to detect VUR using the power received by the antenna. The radiometric antenna for VUR detection requires directional radiation pattern to detect change in kidney temperature 30–40 mm deep from the skin surface. The efficiency of the receive antenna is evaluated in terms of the antenna power ratio received from the target at depth given by,

$$\eta = \frac{\int_{V_c} P_d \, dv}{\int_{V} P_d \, dv}; \quad V_c \in V. \tag{3}$$

In Eqn (3), V_c represents the effective volume of the dilated calyces and renal pelvis inside the kidney with the warm refluxed urine. The ratio of power density η, received from the target at depth to the total power received from the sensing volume provides a measure of directionality of the radiometric antenna inside the tissue load. In this work, η is used to assess the efficiency of the receive antenna and determine radiometer frequency band for VUR detection, and γ is used to improve the antenna power ratio (η) using an optimal dielectric matching layer.

The organization of the paper is as follows. A simplified 3D model of the kidney derived using Avizo® (Visualization Sciences Group) and anatomical features from CT images of 4–6 year old children is used for antenna design/optimization and thermal modeling of the radiometric signal. The power ratio η, calculated over 1–4 GHz for the theoretical antenna with uniform aperture field is used to determine the frequency band and antenna size for a typical VUR situation. Theoretical antenna simulations are used to design a realistic microstrip log spiral antenna. The power efficiency of the log spiral is improved using thin low loss dielectric matching disk between antenna and tissue load. A perfectly conducting cylindrical cup around the antenna and matching layer is proposed to reduce EMI gathered by the antenna from the surrounding. EM simulations are carried out using HFSS (Ansys Inc) to evaluate the effect of the metal cup on antenna power reception. Time domain thermal simulations of the simplified kidney model obtained with Comsol (Comsol Inc) are used to calculate the change in radiometer brightness temperature detectable by the log spiral antenna for warm 15–25 mL urine refluxes. Radiometric signal change detectable by the log spiral for a 3–5°C temperature change at depth is used to determine the minimum detector sensitivity required for VUR detection. Finally, the voltage reflection measurements (S_{11}) of the log spiral antenna studied in this effort are validated in a saline phantom.

2. Methods

2.1 Computational Model

Kidneys are bean shaped organs in the urinary system that primarily extract waste products from blood and regulate salt levels in the body. The two kidneys of the urinary system are located posterior in the abdomen – one below the liver on the right side of the abdomen and

the other below the spleen on the left as shown in Fig 1a. X-ray CT images of abdomen of children aged 4–6 years were used to construct a layered 3D tissue model with 2 mm skin, 5–20 mm fat and 75 mL kidney located 30–40 mm from the surface. Fig 1b shows the simplified kidney model used in the simulations. The dilated calyces and renal pelvis inside the kidneys that receives the refluxed urine was simplified as a single target of varying volume V_c, in the tissue model. Fig 1b shows the simplified 75 mL kidney with 25 mL (V_c) dilated urine collection system obtained from segmentation of the CT images. Cole-Cole dispersion model of biological tissues reported in [26] was used for tissue dielectric properties in the frequency sweep simulations. Saline liquid phantom with 1.25% sodium chloride in deionized water by weight was formulated and validated with human urine dielectric property reported in [21]. Table 1 lists the dielectric measurements of the urine phantom acquired using a commercial coaxial probe (85070E, Agilent Technologies, Santa Clara USA) and network analyzer (E5071C ENA Series, Agilent Technologies). Dielectric measurements of the urine phantom were used in the dispersion model of urine in the simulation study. The thermal properties used for radiometric signal calculations are listed in Table 2.

2.2 Determination of Antenna Aperture and Radiometer Frequency Band

The radiometer frequency band and antenna size for VUR detection were initially determined for the theoretical antenna modeled as a circular aperture of radius r_a, with linearly polarized uniform aperture field distribution $\vec{E}_a$, in an infinite perfectly conducting ground. The ideal antenna radiates into the computational domain represented by a dielectric half space containing the tissue [14,27]. EM frequency domain simulations were carried for an x-polarized uniform electric field in the aperture opening radiating into the dielectric half space, z<0 filled with the layered tissue model of Fig 1b using the finite element simulation software HFSS (Ansys/Ansoft Inc., Pittsburg USA). EM radiation received by the aperture antenna was calculated by solving Maxwell's wave equation [28],

$$\nabla^2\vec{E}(\vec{r},f)+\omega^2\mu_o\varepsilon_o\varepsilon_c(\vec{r},f)\vec{E}(\vec{r},f)=0 \quad (4)$$

with the antenna radiating into the sensing volume (V). In Eqn (4), $\omega = 2\pi f$ is angular frequency, μ_0 and ε_0 are free space magnetic permeability and dielectric permittivity respectively, $\varepsilon_c = \varepsilon_r - j\sigma/\omega\varepsilon_0$ is the complex dielectric permittivity inside V and ε_r is the relative permittivity of the medium. Boundaries of the tissue model are terminated with perfectly matched layer (PML) boundary condition. Fig 2 shows the power density distribution P_d, maintained by an x-polarized aperture field ($\vec{E}_a$) of a 30 mm aperture radius. Simulations were carried out for the theoretical antenna over 1–4 GHz for aperture radius r_a = 20–40 mm, fat layer d_f = 5– 20 mm, target depth d = 35–55 mm, and 15 and 25 mL reflux volumes inside the 75 mL kidney. Power ratio η computed for the parametric variations was used to determine the aperture size (r_a) of the physical antenna and the radiometer frequency band ($f_c \pm \Delta f/2$) for VUR detection.

2.3 Log Spiral Antenna Design

Simulation data of the abstract antenna was used to design a microstrip logarithmic spiral patch antenna with ground plane backing and SMA feed structure for kidney temperature monitoring over $f_c \pm \Delta f/2$. The directional radiation pattern and broadband performance of spirals over multiple octaves make it favorable for deep tissue temperature monitoring. The equation describing the log spiral is defined by [29],

$$\rho=\rho_0 e^{a\varphi} \tag{5}$$

in polar coordinates where, $1/a$ is spiral expansion rate, φ is angular position in radians, ρ_0 is spiral inner radius at $\varphi = 0$ and ρ is 2D position vector at $\theta = \pi/2$ i.e., $z = 0$ plane. The logarithmic spiral (also known as equiangular spiral) defined by the angles in Eqn (5) belongs to the family of frequency independent antennas with directional radiation pattern. The frequencies supported by a finite length log spiral is a function of its arm length given by [29],

$$L=(\rho_1 - \rho_0)\sqrt{1+1/a^2} \tag{6}$$

where, ρ_1 is spiral outer radius. The single arm log spiral studied in this effort was defined by a curved surface with edges $\rho_{e1} = \rho_0 e^{a\varphi}$ and $\rho_{e2}=\rho_0^{'} e^{a\varphi}$ where, $\rho_0^{'}=\rho_0 e^{-a\varphi_0}$ and $e^{-a\varphi 0}<1$. The outermost radius of the spiral was limited to r_a, determined from the simulations of the theoretical antenna described in section 2.2.

The conducting arm of the microstrip log spiral antenna was simulated on a 1.524 mm thick hydrocarbon ceramic substrate (RO4350B, Rogers Corp. USA) with dielectric constant, $\varepsilon_r = 3.66$ and $\tan\delta = 0.0037$ over the frequency range of interest. The design parameters (a, ρ_0) were chosen to support frequencies $f_c \pm \Delta f/2$ for the spiral outer radius (ρ_1) determined from the theoretical antenna simulations. The single arm log spiral antenna was fed by a SMA connector with the center conductor of the coaxial line connected to the conducting arm of the spiral through a microstrip via hole in the dielectric substrate. The outer conductor of the SMA was connected to the ground plane behind the substrate. Full wave simulations were carried out for waves launched inside the coaxial line feeding the SMA conductor using HFSS to determine radiation pattern and scattering parameters for the several parametric scenarios.

2. 4 Radiometric Efficiency of Log Spiral Antenna

A thin low loss dielectric disk was used between the antenna and tissue load to improve EM coupling (γ) and the power received by the physical antenna from the target at depth (η). Simulations were carried out for 0.25 and 1 mm thick (d_{ml}) dielectric disks of radius r_a and relative permittivity (ε_r) ranging from 3–30 with 0.004 loss tangent. Dielectric property of the matching layers studied in the simulations is based on the commercially available Eccostock® dielectric disks (Emerson & Cuming Microwave Products USA). The matching layer that yielded maximum η over $f_c \pm \Delta f/2$ was used in the radiometer brightness temperature calculations for the microstrip log spiral antenna.

The extremely low thermal noise power received by the log spiral antenna on the order of 10^{-20} W/Hz is susceptible to EMI from the surrounding environment. Thus, a cylindrical metal cup surrounding the antenna and matching layer was proposed to shield the low power signal gathered by the receive antenna from external EMI picked up from the edges of the antenna substrate. Simulations were carried out to study the effect of the shield cup on antenna power reception. In the computational model, the metal cup surrounding the antenna and matching layer was in complete contact with the antenna ground plane and the skin surface. The continuous contact protects the substrate exposed on the antenna periphery from potential EMI. The power ratio (η) of the log spiral with a matching layer inside the shield cup was studied for 25 mL urine reflux inside the kidney located 35 mm from the skin surface. The height of the metal cup was set to 60 mm, tall enough to house the antenna,

matching layer and receiver components to provide EM shielding to the antenna as well as the receiver front end.

2.5 Radiometric Signal Change Detectable by Log Spiral Antenna

Theoretical evaluation of the Pennes bio-heat transfer equation compared to other heat transfer models that account for convection and realistic anatomy of perfused kidney indicated good agreement with less than 0.5°C deviation in pig kidneys [30]. Thus, thermodynamics inside the kidney and tissue load are approximated using Pennes bio-heat equation [30],

$$\rho C_p \frac{\partial T}{\partial t} + \nabla \cdot (-k_t \nabla T) - \omega_b c_b (T_a - T) + Q_{met} = 0 \tag{7}$$

for simplicity. In Eqn (7), k_t is tissue thermal conductivity, T is tissue temperature inside the computational domain V, T_a is arterial blood temperature, ω_b and c_b are perfusion rate and specific heat capacity of blood respectively, ρ is tissue density and C_p is tissue specific heat capacity, and Q_{met} is the negligible heat generated due to metabolic activity that was neglected in this realistic but simplified model. The spatial dependence of the variables was dropped in Eqn (7) for simplicity. Temperature on the tissue boundary at depth was set to body core temperature of 37°C. Temperature on the skin surface was subjected to convective heat transfer boundary condition $\hat{n} \cdot k_t \nabla T = h_a (T_r - T)$, where, $\hat{n}$ is the normal vector on the boundary surface, h_a is effective heat transfer coefficient and T_r is ambient room temperature. The remaining tissue boundaries were subjected to support normal heat flux from the body core to the skin surface.

Urine reflow from the warm bladder maintained at 40–45°C experiences heat loss to the surrounding tissues at body core temperature of 37°C. Thus, the refluxed urine temperatures were studied for 40–42°C. The rate at which the temperature of the warm urine reaches thermal equilibrium with the surrounding kidney tissue is a complex convection phenomenon which is beyond the scope of this paper. This complex heat transfer was approximated by bulk heat exchange between the reflux volume (V_c) at a constant temperature and the surrounding kidney tissue using Penne's bio-heat equation where V_c represents the aggregate volume of the dilated renal pelvis and calyces inside the 75 mL kidney. The rate at which the urine reaches 37°C after reflux was studied for the varying homogeneous reflux temperature distributions inside V_c shown in Fig 3. In Fig 3, $T_{15}^{1}(t)$ and $T_{15}^{2}(t)$ represent two possible temperature exchange with the surrounding kidney tissue for the 15 mL reflux at 40°C peak reflux temperature. Note that the 25 mL refluxes at 40°C denoted by $T_{25}^{1}(t)$ and $T_{25}^{2}(t)$ in Fig 3 lose heat slower than their counterparts ($T_{15}^{1,2}(t)$) due to larger thermal mass. Likewise, the 15 mL reflux at 42°C ($T_{15}^{3,4}(t)$) reaches 37°C slower than the 40°C refluxes ($T_{15}^{1,2}(t)$) due to higher urine inlet temperature. Varying urine temperature distributions were studied to account for the possible variations in the heat transfer phenomena. The steady state tissue temperature calculated for V_c at arterial blood temperature of 37°C was used as the initial value for the transient simulations. Thermal modeling of the warm reflux was studied using the finite element simulation software Comsol (Comsol Inc. Stockholm, Sweden). The finite element model had 124511 elements out of which the 75 mL kidney had 13000 elements. The thermal simulations were performed using an iterative solver with 1e-4 error. Transient thermal simulations were carried out for the tissue properties in Table 2 to calculate the radiometer brightness temperature change,

$$\delta T_B(\vec{r}, t) = T_B(\vec{r}, t^+) - T_B(\vec{r}, t^-) \quad (8)$$

detectable by the log spiral antenna for reflux volumes V_c = 15, 25 mL at 40–42°C located 35 mm from the skin surface. In (8), $T_B(\vec{r}, t^-)$ is the radiometer state before warm reflux and $T(\vec{r}, t^+)$ is the transient response during reflux. The change in antenna brightness temperature (δT_B) calculated for different reflux volumes and urine temperatures was used to estimate the sensitivity of the radiometer receiver for VUR detection.

2.6 Antenna Measurements

The tapered log spiral antenna studied in this effort was fabricated on a 1.524 mm thick hydrocarbon ceramic substrate (RO4350B, Rogers Corp. USA) for the exact design parameters used in the simulations. A liquid phantom with 6 [g/L] salt (NaCl) in deionized water was used to validate antenna simulation data with measurements. Dielectric property of the saline phantom was measured over 1–4 GHz using Agilent's dielectric probe kit (85070E, Agilent Technologies, Santa Clara USA). A simple numerical model was created in the EM simulation software to calculate antenna S_{11} data for the saline phantom using the measured dielectric property for model validation.

3. Results

3.1 Antenna Aperture and Radiometer Frequency

Fig 4 shows the % power ratio (η) curves of the theoretical antenna for varying aperture radius and tissue load with 25 mL (V_c) urine reflux inside the kidney. The target depth from the skin surface is 37 and 42 mm respectively for the tissue load with 5 and 10 mm fat layer. Comparison of the power ratio (η) curves indicate that lower power is received from deeper targets and smaller apertures. Fig 4 also shows that η is a non-monotonic function of frequency and aperture radius and it reaches the maximum over 1–2 GHz for r_a: 30–40 mm. Similar curves were obtained for the y-polarized plane wave (simulation data not shown). However, as per the frequency allocation chart of Federal Communications Commission (FCC), a government agency in United States of America, 800–960 MHz and 1710–2100 MHz are allocated for GSM 800, 1800/1900 and 3G cellular communications. The simulation data of Fig 4 and FCC guidelines were used to select 1.1–1.6 GHz frequency band for radiometry and a receive antenna with aperture radius 30–40 mm for VUR detection.

3.2 Microstrip Log Spiral Antenna for VUR Detection

Tapered Log Spiral—Fig 5 shows the microstrip log spiral antenna with parameters, a = 0.11 [1/radian], ρ_0 = 3 mm, $\rho_0' = 2.1$ mm and $\varphi_0 = \pi$ designed based on the power ratio curves of the theoretical antenna. The 35 mm radius self complementary antenna of Fig 5 has directional radiation pattern over 1.1–1.6 GHz and broadband spectral response over 1–4 GHz. Substituting the antenna design parameters into Eqn (6) yields the lower bound on the operating frequency as 970 MHz. In the simulations, the antenna arm was tapered as shown by the dotted lines in Fig 5 for matched termination. Tapering the antenna arm minimizes reflections at lower frequencies and improves load matching. The lowest frequency supported by the tapered log spiral antenna of Fig 5 is 660 MHz. The back ground plane assures unidirectional radiation pattern and good but incomplete protection from EMI (due to exposed substrate edges).

Dielectric matching layer for improved power reception—Fig 6 shows the antenna reflection coefficient and power ratio curves of the tapered log spiral antenna over 1.1–1.6

GHz for the 0.25 and 1 mm matching layers of several dielectric permittivities between the antenna and tissue load. The tissue load has 2 mm skin, 5 mm fat and kidney with 25 mL urine located 40 mm deep. It can be observed in Fig 6 that as the reflection coefficient ($|S_{11}|$) decreases, power received by the log spiral antenna from the deep target (η) increases. The 1 mm matching layer of $\varepsilon_r = 3$ improved EM coupling to the tissue load leading to enhanced power transmission ($\gamma = 1 - |S_{11}|^2$) and power ratio (η). This is clearly demonstrated in the normalized power density depth profiles of Fig 7 calculated in the presence and absence of the 1 mm matching layer of $\varepsilon_r = 3$.

Comparison of the power ratio curves of the theoretical (Fig 4) and physical (Fig 6) antennas indicate that much less power is gathered by the practical microstrip log spiral antenna. The power received by a physical antenna from the target at depth is only 2–4% for the 25 mL target and is expected to be lower for low reflux volumes (10–15 mL). Furthermore, the difference in the power received due to the localized temperature change inside the well perfused kidneys during warm reflux is expected to be negligible as the tissue dielectric properties remain almost the same over the narrow temperature window of 37–42°C i.e., $W(\vec{r}, f)^{reflux} \approx W(\vec{r}, f)^{noreflux}$. Thus, the radiometer brightness temperature change (δT_B) for VUR detection is expected to be predominantly dependent on the localized temperature change inside the kidneys.

Effect of shield cup on antenna power reception—Fig 8a shows the power ratio received by the log spiral antenna from 25 mL urine 35 mm deep with and without a cylindrical metal cup surrounding the antenna and matching layer (1 mm and $\varepsilon_r = 3$) as shown in computational model of Fig 8b. Comparison of the curves indicates that the power received by the log spiral antenna from the target at depth increased from 2–4% to 5–6% over 1.1–1.6 GHz in the presence of the shield cup. Thus, the metal cup surrounding the antenna and matching layer in continuous contact with antenna ground plane and the skin surface intended to reduce EMI picked up the antenna did not deteriorate the power received from the target at depth. The increased power reception observed for the EM shielded microstrip log spiral is currently under investigation, but it is probably due to reduced loss of signal at the shielded edge of the substrate.

3.3 Radiometric Signal Change during Warm Reflux

Fig 9 shows the transient temperature distribution in the mid section of the kidney for warm 15 mL reflux at temperature, $T_{15}^{4}(t)$ (refer Fig 3). The outer and inner contours of Fig 9 indicate the boundaries of the kidney and 15 mL reflux respectively. In Fig 9, the 15 mL urine at 42°C quickly lost temperature (<30 s) to the surrounding kidney tissue with very high blood perfusion (refer Table 1). Fig 10a shows the change in radiometric brightness temperature detectable by the log spiral antenna for the warm 15 mL reflux calculated over the radiometric frequency band (1.1–1.6 GHz). The radiometric temperature calculations of Fig 10a were performed using Eqns (1, 4, 7–8) for 1 mm matching layer of $\varepsilon_r = 3$ and the refluxed urine temperatures of Fig 3. It should be noted that, a 3–5°C temperature change inside the kidney located 35 mm deep resulted only in a small change of 0.10 – 0.17 K in the radiometer brightness temperature. The change in volume average tissue temperature δT_B, detectable by the log spiral antenna for a 15 mL urine reflux is smaller for lower urine temperatures ($T_{15}^{1,2}(t)$ versus $T_{15}^{3,4}(t)$ in Fig 10a).

Fig 10b shows the change in radiometric signal sensed by the log spiral antenna over 1.1–1.6 GHz for 25 mL reflux at 40°C and 35 mm deep from the skin surface calculated in the presence and absence of the cylindrical shield cup. The variation in brightness temperature change (δT_B) is 0.125 K without shield cup and 0.175 K with the antenna and matching layer inside the shield cup. Larger radiometric signal change detected with the shield cup is

due to higher power received by the antenna from the target at depth in the presence of the metal shield cup (Fig 8). From Fig 10, it should also be noted that the radiometric signal change is higher for larger reflux grades (15 versus 25 mL at 35 mm depth). The delay in the peak brightness temperature observed in Fig 10 is due to heat diffusion from the warm refluxed urine to the surrounding kidney tissues (Fig 9) which increases the apparent thermal volume of the target sensed by the receive antenna. Radiometer brightness temperature change detectable by the log spiral antenna suggests a receiver with detector sensitivity better than 0.1 K for VUR detection.

3.4 Antenna Measurements

Fig 11 compares antenna S_{11} measurements with simulation data for the saline phantom. The 35 mm radius tapered microstrip log spiral antenna in Fig 11 is fabricated on a 1.524 mm thick hydrocarbon ceramic substrate (RO4350B, Rogers Corp. USA) of ε_r = 3.66 and 0.0037 loss tangent for the design parameters of Fig 5. Fig 11 shows very good agreement between simulation and measurement data of the microstrip log spiral antenna designed for passive kidney temperature monitoring. It is thus expected that the simulation results obtained for complex scenarios are accurately predicting the power deposition patterns in future clinical cases.

4. Discussion

A MW diagnostic system with 915 MHz antenna array for external bladder warming to fever range temperatures (40–45°C) and a radiometer for passive temperature monitoring was recently reported for noninvasive detection of warm reflux in kidneys [11]. Due to high blood perfusion inside the kidneys, transient temperature change during warm reflux is expected to last less than a minute at depth. Thus, a single band low frequency radiometer was studied for noninvasive kidney temperature monitoring to detect the fast temperature change at depth. Furthermore, detecting the warm reflux at depth requires a receive antenna with high directional sensitivity and good coupling to a range of tissue load – varying thickness fat and muscle tissues and reflux volumes at different temperatures.

CT images of children ages 4–6 years were used to determine the volume and location of kidney and the thickness range of skin, fat and muscle tissues to build a simplified 3D model. The antenna design and radiometer frequency selection were carried out based on the ratio of power received by the radiometric antenna from the target at depth η, defined in Eqn (3). The power ratio plays an important role in antenna brightness temperature measurement as evidence in Eqn (1) and rewritten below for clarity,

$$T_{B,i}(\vec{r},t)=\int_{BW}\gamma df\left(\frac{\int_{V-V_c}P_d(\vec{r}',f)T(\vec{r}',t)dv+\int_{V_c}P_d(\vec{r}',f)T(\vec{r}',t)dv}{\int_{V}P_d(\vec{r}',f)dv}\right)+T_{EMI}+T_{sys};\quad r\notin V. \tag{9}$$

From Eqn (9), it can be observed that a receive antenna with higher η over the i^{th} frequency band is desirable for radiometric sensing. An antenna with uniform aperture field in an infinitely long ground plane radiating into a half space filled with the layered tissue model was studied as a general ideal case. Such an abstract radiator is often used in antenna theory and computational studies to generate the theoretical radiation patterns and estimate the optimal parameters for the design of a physical antenna [14,27]. Thus, the power ratio received by the ideal antenna from the target inside the kidneys (η) was used in our case to determine the optimal frequency band and center frequency of the radiometer (f_c, Δf) and

aperture size of the physical antenna (r_a) for VUR detection. Temperature dependence of EM tissue property was neglected in the simulations as the change in tissue property during warm urine reflux of 15–25 mL at 40–42°C inside the well perfused kidneys receiving 20–25% of the cardiac blood flow at 37°C is expected to be minimal.

The power ratio curves of Fig 4 calculated for the linearly polarized uniform aperture indicated higher η for larger aperture radius. However, the power ratio was not a monotone function of frequency and aperture size. The power ratio was relatively higher over 1–2 GHz and was maximum for r_a over 30–40 mm. An important observation in Fig 4 is that the power received by the theoretical antenna from the target at depth is only 2–7% of its total power and passive kidney temperature monitoring using MW radiometry involves sensing the change in very low power EM radiation. Based on the power ratio curves and FCC frequency allocation chart, a MW radiometer with 1.1–1.6 GHz frequency band (f_c = 1.35 GHz, Δf = 500 MHz) and receive antenna with aperture radius 30–40 mm was used to design a physical patch antenna for passive kidney temperature monitoring.

Subsequently, a microstrip log spiral patch antenna with circular polarization was designed for VUR detection. The single arm spiral patch antenna with ground plane backing on a low loss printed circuit board (PCB) substrate (1.524 mm thickness) was chosen for its low profile, simple feed and ability of the ground plane to shield EMI from the surrounding. The design parameters of the 35 mm radius log spiral antenna of Fig 5 (a, ρ_0, ρ_1, L, φ_0) were determined to support directional radiation pattern over 1.1–1.6 GHz. The power received by the log spiral from the target at depth was improved using low loss dielectric matching layer (Fig 6). The dielectric matching layer improved EM coupling (γ) and increased antenna power ratio η, from 1 to 4% (Fig 6). Ultra low loss thin dielectric matching disk (Eccosorb®, Emmerson Cummings, Randolph, MA USA) was used with the log spiral antenna in the preliminary animal study reported in [11] for VUR detection. The use of dielectric filling material to enhance the received low power signal was also investigated for radiometric brain temperature monitoring [31]. It should be noted that the power ratio curves of the physical antenna in Figs 6, 8 are lower compared to the theoretical antenna (Fig 4). This is because the field maintained by the log spiral on the metal patch is non-uniform and limited to the non-metallic region of the patch. Nonetheless, radiometric efficiency of the log spiral antenna is higher for shallow and larger volume targets (Fig 6) as expected and similarly to what is obtained with the theoretical antenna in Fig 4. In addition to matching layer, we also propose EM shielding of the antenna and radiometer to avoid EMI from the surrounding environment. EM simulations indicated no deterioration in antenna power reception in the presence of metal shield cup (Fig 8). The increase in power ratio calculated in the presence of metal cup is currently under investigation. The measurements of the tapered log spiral fabricated based on the simulations are in very good agreement with the simulated data (Fig 11).

Thermal modeling of the antenna brightness temperature change calculated for warm urine reflux (Fig 3) indicated higher δT_B for larger volume (15 vs. 25 mL) and higher urine temperatures (40 vs. 42°C) in Fig 10. Furthermore, δT_B was calculated to be higher in the presence of shield cup due to the increased power received by the log spiral from the target (5–6% compared to 2–4% in Fig 8). Radiometer brightness temperature change of 0.1 K calculated for a 15 mL reflux at 3°C above the kidney core temperature (Fig 10) indicates that the MW radiometer should have less than 0.1 K sensitivity for VUR detection. The receiver sensitivity is the standard deviation of the radiometer brightness temperature measured by the antenna and is given for a total power radiometer by [13],

$$\delta T = \frac{T_A + T_N}{\sqrt{B \cdot \tau}} \tag{10}$$

assuming negligible system gain variation ($\Delta G = 0$) during signal acquisition. In Eqn (10), τ is signal integration time, T_A is antenna brightness temperature, $T_N = T_0 (NF - 1)$ is system noise temperature where $T_0 = 293$ K is room temperature and NF is receiver noise figure. The detector sensitivity of a Dicke radiometer in the absence of signal drift is approximately twice that of the total power radiometer ($\delta T_D \approx 2\ \delta T$) [13]. Table 3 lists the theoretical detector sensitivity of a MW radiometer system with 500 MHz receiver bandwidth for T_A = 300 K (antenna on skin) and various noise figures and integration times. From Table 3, it can be observed that higher sensitivity can be obtained for a receiver with lower noise figure and larger signal acquisition time. However, larger signal acquisition is not desirable to detect the fast temperature change during reflux. EM and thermal simulations of the microstrip log spiral antenna suggest a single band low frequency MW radiometer centered at 1.35 GHz with 500 MHz bandwidth, low receiver noise figure and detector sensitivity significantly better than 0.1 K could be used for passive detection of the warm reflux inside the kidneys. The MW radiometer used in the animal study reported in [11] for noninvasive VUR detection was designed based on this theoretical modeling effort and has demonstrated 0.03 K detector sensitivity in preclinical testing. The influence of antenna positioning error and internal organ motion on radiometric signal detection will be investigated in the upcoming clinical feasibility studies of this system.

5. Summary and conclusion

This study identifies the optimal radiometer frequency band for passive temperature monitoring of kidney during VUR, estimates the required receiver sensitivity with thermal modeling of warm urine refluxing from bladder to kidney, and presents the design of an efficient radiometric receive antenna capable of sensing thermal emissions from deep in the body. The ratio of power received from a small target volume at depth to the entire power received by a theoretical antenna aperture is considered along with FCC guidelines to design a 35 mm radius tapered microstrip log spiral antenna with directional radiation pattern over 1.1–1.6 GHz. A thin low loss dielectric matching layer is used to improve antenna impedance matching to the layered fat/muscle/kidney load and the power received from the kidney target at depth. A metal cup surrounding the antenna is proposed to shield the low power signal gathered by the receive antenna from external EMI. Radiometric brightness temperature calculations from the power received by the log spiral antenna for reflux of 15 or 25 mL of 40–42°C urine located 35 mm deep suggest the need for a detector with sensitivity less than 0.1 K for a 1.35 GHz radiometer with 500 MHz band width for VUR detection. Scattering measurements of the tapered microstrip log spiral antenna on a realistic phantom indicate good agreement with the design/simulation data. From these studies, we conclude that the tapered log spiral antenna with metal cup for EM shielding should receive sufficient power from the target at depth which could be fed to a radiometer with better than than 0.1 K sensitivity designed over 1.1–1.6 GHz to accurately detect the 40–42°C reflux of 15–25 mL urine into the calyces at a depth of 35 mm.

Acknowledgments

This research effort was supported by ThermImage Corporation, Salt Lake City USA. The authors would like to thank Michael Hoffman and Stan Mills at Agilent Technologies, Bob Helsby and Dane Thomson at Ansys/Ansoft Corporation and Bill Henderson at Avizo Visualization Sciences Group for their generous technical and license support.

References

1. Bailey, R. An overview of reflux nephropathy. New York: Masson; 1979. p. 3-13.
2. Hellstrom M, Jacobsson B, Marild S, Jodal U. Voiding cystourethrography as a predictor of reflux nephropathy in children with urinary tract infection. American Journal of Roentgenology. 1989; 152(4):801–804. [PubMed: 2784263]
3. Sargent MA. What is the normal prevalence of vesicoureteral reflux? Pediatric Radiology. 2000; 30(9):587–593. [PubMed: 11009294]
4. Smellie J, Normand I, Katz G. Children with urinary tract infection: a comparison of those with and those without vesicoureteric reflux. Kidney Int. 1981; 20:717–722. [PubMed: 7334746]
5. Pediatrics AA. Practice parameter: the diagnosis, treatment, and evaluation of the initial urinary tract infection in febrile infants and young children. Pediatrics, Committee on Quality Improvement, Subcommittee on Urinary Tract Infection. 1999; 103:843–852.
6. Brenner DJ, Elliston CD, Hall EJ, Brendon WE. Estimated risks of radiation-induced fatal cancer from pediatric CT. American J Roentgenology. 2001; 176:289–296.
7. Traxel E, DeFoor W, Reddy P, Sheldon C, Minevich E. Risk factors for urinary tract infections after dextranomer/hyaluronic acid endoscopic injection. Journal of Urology. 2009; 182:1708–1713. [PubMed: 19692024]
8. Frush DP, Donnelly LF, Rosen NS. Computed tomography and radiation risks: what pediatric health care providers should know. Pediatrics. 2003; 112(4):951–957. [PubMed: 14523191]
9. Kirsch A, Grattan-Smith J, Molitierno J. The role of magnetic resonance imaging in pediatric urology. Current Opinion in Urology. 2006; 16:283–290. [PubMed: 16770129]
10. Darge K, Troeger J. Vesicoureteral reflux grading in contrast-enhanced voiding urosonography. Eur J Radiol. 2002; 43:122–128. [PubMed: 12127209]
11. Snow W, Taylor M. Non-Invasive Vesicoureteral Reflux Imaging. 2010 accepted in J Pediatric Urology.
12. Land DV. An efficient, accurate and robust radiometer configuration for microwave temperature measurement for industrial and medical applications. Journal of microwave power and electromagnetic energy. 2001; 36(3):139–153. [PubMed: 11837048]
13. Ulaby, FT.; Moore, RK.; Fung, AK. Microwave Remote Sensing Fundamentals and Radiometry. Vol. I. Artech House; 1981. Microwave Remote Sensing, Active and Passive.
14. Bardati F, Iudicello S. Modeling the Visibility of Breast Malignancy by a Microwave Radiometer. IEEE Transactions on Biomecial Engineering. 2008; 55(1):214–221.
15. Mouty S, Bocquet B, Ringot R, Rocourt N, Devos P. Microwave radiometric imaging (MWI) for the characterisation of breast tumours? The European Physical Journal Applied Physics. 2000; 10:73–78.
16. Hand JW, Van Leeuwen GMJ, Mizushina S, Van de Kamer JB, Maruyama K, Sugiura T, Azzopardi DV, Edwards AD. Monitoring of deep brain temperature in infants using multi-frequency microwave radiometry and thermal modelling. Physics in Medicine and Biology. April. 2001 46:1885–1903. [PubMed: 11474932]
17. Maruyma K, Mizushina S, Sugiura T, Leeuwen GMJV, Hand JW, Marrocco G, Bardati F, Edwards AD, Azzopardi D, Land D. Feasibility of Noninvasive Measurement of Deep Brain Temperature in Newborn Infants by Multifrequency Microwave Radiometry. IEEE Trans Microwave Theory ans Techniques. November; 2000 48(11):2141–2147.
18. Ohba H, Kinomura M, Ito M, Sugiura T, Mizushina S. Multifrequency microwave radiometry for non-invasive thermometry using a new temperature profile model function. IEICE Transactions on Electronics. 1995; E78-C(8):1071–81.
19. Arunachalam K, Stauffer PR, Maccarini PF, Jacobsen S, Sterzer F. Characterization of a digital microwave radiometry system for noninvasive thermometry using a temperature-controlled homogeneous test load. Physics in Medicine and Biology. 2008; 53(14):3883–3901. [PubMed: 18591733]
20. Camart JC, Despretz D, Prevost B, Sozanski JP, Chive M, Pribetich J. New 434 MHz interstitial hyperthermia system monitored by microwave radiometry: theoretical and experimental results. International Journal of Hyperthermia. 2000; 16(2):95–111. [PubMed: 10763740]

21. Dietsch A, Camart JC, Sozanski JP, Prevost B, Mauroy B, Chive M. Microwave Thermochemotherapy in the Treatment of the Bladder Carcinoma—Electromagnetic and Dielectric Studies—Clinical Protocol. IEEE Transactions on Biomedical Engineering. 2000; 47(5):633–641. [PubMed: 10851807]
22. Jacobsen S, Stauffer PR, Neuman DG. Dual-mode antenna design for microwave heating and noninvasive thermometry of superficial tissue disease. IEEE Transactions on Biomedical Engineering. 2000; 47(11):1500–9. [PubMed: 11077744]
23. Karanasiou IS, Karathanasis KT, Garetsos A, Uzunoglu NK. Development and Laboratory Testing of a Noninvasive Intracranial Focused Hyperthermia System. IEEE Transactions on Microwave Theory and Techniques. 2008; 56(9):2160–2171.
24. Karanasiou IS, Papageorgiou C, Uzunoglu NK. Is it possible to measure non-invasively brain conductivity fluctuations during reactions to external stimuli with the use of microwaves? International Journal of Bioelectromagnetism. 2005; 7(1):356–359.
25. Jacobsen S, Klemetsen O. Improved Detectability in Medical Microwave Radio-Thermometers as Obtained by Active Antennas. IEEE Transactions on Biomedical Engineering. 2008; 55(12):2778–2785. [PubMed: 19126458]
26. Gabriel S, Lau RW, Gabriel C. The dielectric properties of biological tissues: III. Parametric models for the dielectric spectrum of tissues. Physics in Medicine and Biology. 1996; 41:2271–2293. [PubMed: 8938026]
27. Balanis, CA. Antenna Theory: Analysis and Design. 2. New York: John Wiley & Sons, Inc; 1982.
28. Pozar, DM. Microwave engineering. John Wiley & Sons; 2004.
29. Dyson JD. The Equiangular Spiral Antenna. IRE Transactions on Antennas and Propagation. 1959; AP-7:181–187.
30. Xu LX, Chen MM, Holmes KR, Arkin H. The theoretical evaluation of the Pennes, the Chen-Holmes and the Weinbaum-Jiji bioheat transfer models in the pig renal cortex. Advances in Biological Heat and Mass Transfer ASME. 1991:15–21. vol. HTD Vol. 189/BED Vol. 18.
31. Karathanasis, KT.; Gouzouasis, IA.; Karanasiou, IS.; Uzunoglu, NK. Simulation and Experimental Study of an Ellipsoidal Cavity Reflector as part of a Focused Passive Brain Imaging System. In: Sloten, JV.; Verdonck, P.; Nyssen, M., et al., editors. IFMBE Proceedings. Springer; Berlin Heidelberg: 2009. p. 1565-1569.
32. Bernardi P, Cavagnaro M, Pisa S, EPE. Specific absorption rate and temperature elevation in a subject exposed in the far-field of radio-frequency sources operating in the 10–900-MHz range. IEEE Trans Biomed Eng. 2003; 50:294–304.
33. Holmes, KR. Thermal properties. 2009. http://users.ece.utexas.edu/~valvano/research/Thermal.pdf
34. Van de Kamer JB, Van Wieringen N, De Leeuw AAC, Lagendijk JJW. The significance of accurate dielectric tissue data for hyperthermia treatment planning. Int J Hyperthermia. 2001; 17(2):123–142. [PubMed: 11252357]

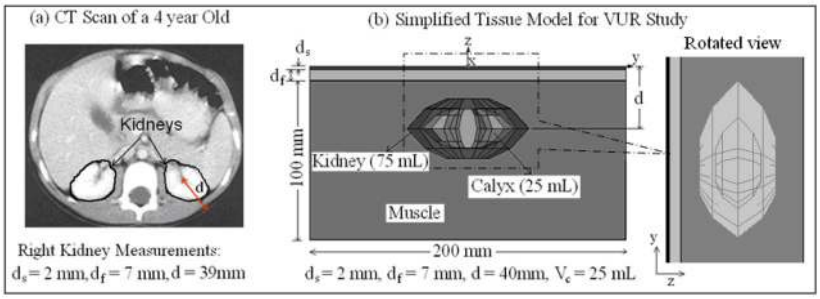

Fig 1.

(a) CT scan of a 4 year old in the axial plane; distance from the center of the kidney to skin surface is 39 mm (b) Simplified 3D tissue model used in the numerical simulations based on average tissue measurements obtained from CT scans of children ages 4–6 years.

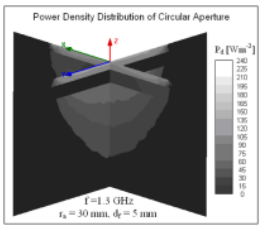

Fig 2.

Power density in the orthogonal planes across the various tissue layers at 1.3 GHz calculated for an x-polarized uniform aperture field ($\vec{E_a}$) in the absence of kidney.

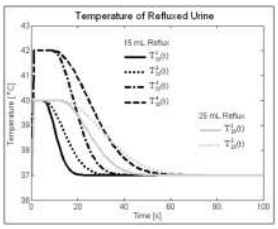

Fig 3.

Urine temperature used in thermal simulations to model reflux of warm urine from bladder to kidney followed by rapid heat loss to the surrounding well perfused kidney. Urine reflux temperature were modeled for varying reflux volumes (15, 25 mL) and urine temperatures (40–42°C) to model the possible heat transfer phenomena inside the perfused kidney tissues during reflux of warm urine.

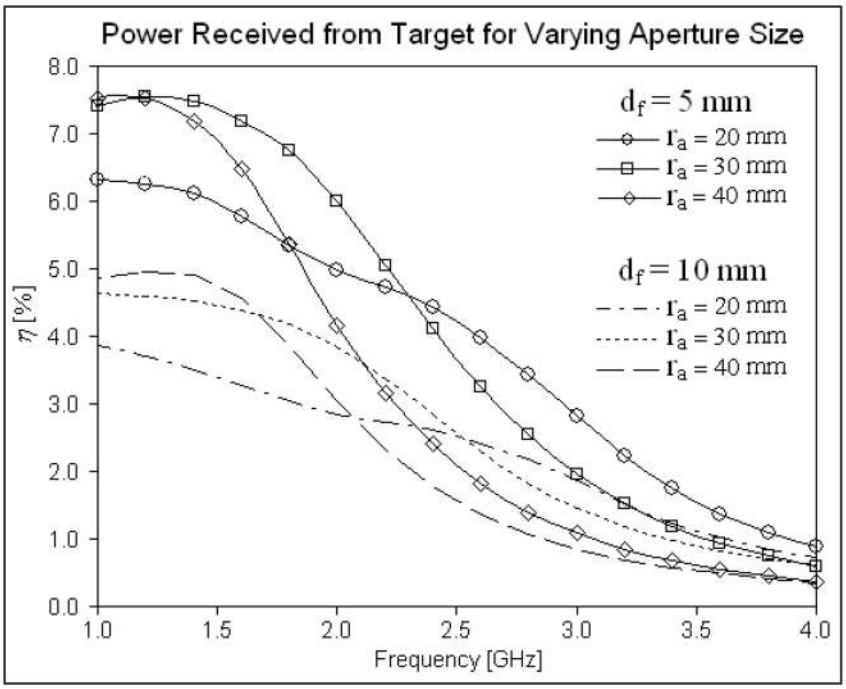

Fig 4.

Power ratio (η) curves calculated for varying aperture radius of the theoretical antenna radiating into the layered tissue load with 5 and 10 mm fat layer and 25 mL urine inside 75 mL kidney. The target depth from skin surface is 37 and 42 mm respectively for the tissue load with 5 and 10 mm fat layer. Note that the theoretical antenna receives only 4–8% of the total power from the target at depth over 1–2 GHz and less than 4% for frequencies above.

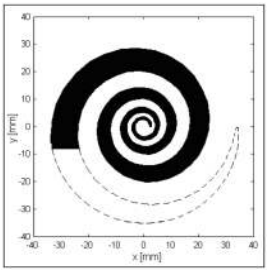

Fig 5.

The 35 mm radius tapered microstrip log spiral antenna with directional radiation pattern over the radiometric frequency band (1.1–1.6 GHz) optimally designed for VUR detection. The shaded arms are from Eqn (5) with 35 mm outer spiral radius. The dashed lines indicate the tapering obtained by extending the spiral edges beyond 35 mm radius and intersecting with a 35 mm radius circle. The antenna is backed by a ground plane and fed by the center conductor of an SMA connector.

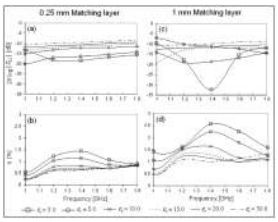

Fig 6.

Parametric simulations to improve the ratio of power received from the 40 mm deep target by the tapered log spiral antenna using thin low loss dielectric matching layer. (a) Antenna reflection coefficient and (b) power ratio curves for 0.25 mm matching layer; (c) antenna reflection coefficient and (d) power ratio curves for 1 mm matching layer. Lower $|S_{11}|$ obtained for 1 mm matching layer of ε_r = 3.0 yielded higher η (1.5–3%) over 1.1–1.6 GHz.

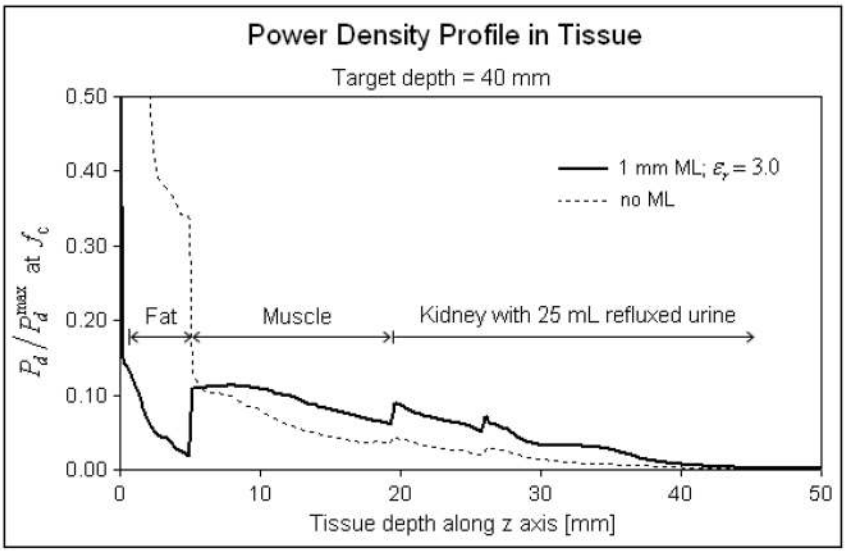

Fig 7.

Normalized tissue power density depth profiles calculated for the log spiral antenna at radiometer center frequency (1.35 GHz) in the presence and absence of matching layer. The low loss dielectric matching layer significantly increased power received by the log spiral antenna from the 25 mL target at depth.

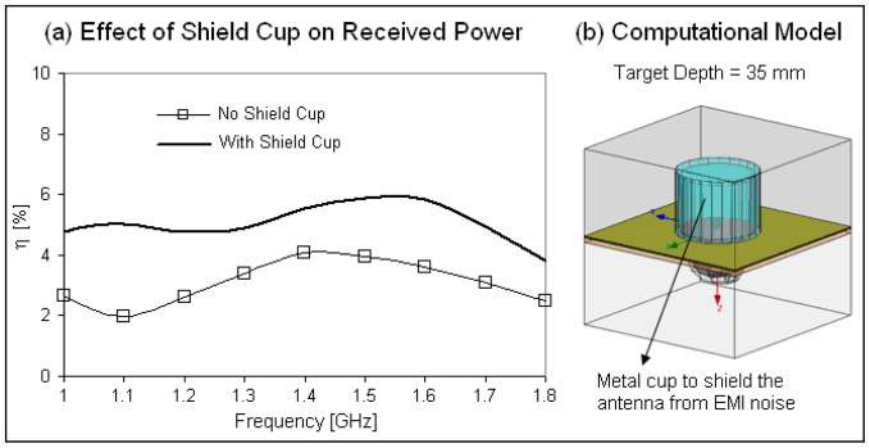

Fig 8.

(a) Effect of shield cup on the ratio of power received by the log spiral antenna from 25 mL target located 35 mm from the skin surface (b) 3D computational model showing the cylindrical cup surrounding the antenna and matching layer. The metal cup is in continuous contact with the antenna ground plane and skin surface in Fig 9b. No deterioration was observed in the power received by the antenna inside the shield cup. Increased power reception noted in the presence of shield cup is being investigated but it is probably due to reduced loss of signal at the shielded edge of the substrate.

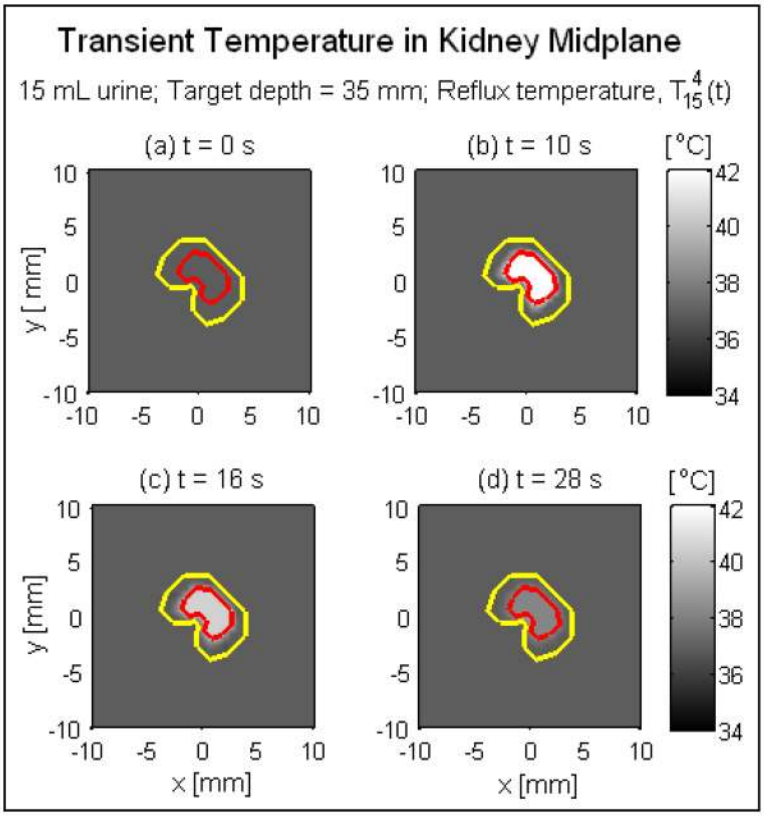

Fig 9.

Transient temperature field in the kidney mid plane for 15 mL warm urine reflux at $T_{15}^4(t)$ (Fig 3) located 35 mm deep from the skin surface. The contours outline the kidney (outer) and 15 mL warm urine reflux (inner).

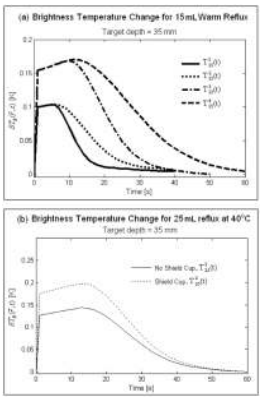

Fig 10.

Radiometer brightness temperature change detectable by the log spiral for warm reflux at fever temperatures (40–42°C) located 35 mm deep from the skin surface calculated for 1 mm matching layer of $\varepsilon_r = 3$ between the antenna and tissue load. (a) δT_B for 15 mL reflux at 40–42 °C, $T_{15}^{j}(t) \forall\ j=1,2,3,4$. (b) δT_B for 25 mL urine reflux at $T_{25}^{2}(t)$ with peak urine temperature at 40°C calculated in the presence and absence of the metal cup surrounding the antenna and matching layer. Radiometer brightness temperature change suggests a receiver with detector sensitivity better than 0.1 K will be required for VUR detection. Higher δT_B could be obtained in the presence of shield cup in addition to being not susceptible to EMI from the surrounding.

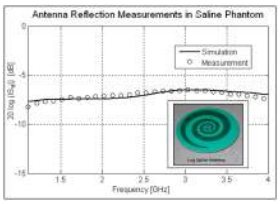

Fig 11.

Comparison of the simulation and experimental antenna reflection data, $|S_{11}|^2$ obtained for the tapered microstrip log spiral antenna in saline phantom (6 [g/L] salt in deionized water). Measurements in saline phantom are used to validate the EM simulations presented in this work. The log spiral antenna of Fig 11 is fabricated on 1.524 mm thick hydrocarbon ceramic substrate (RO4350B, Rogers Corp. USA) of ε_r = 3.66 and 0.0037 loss tangent for the design parameters of the antenna used in the simulation study (Fig 5).

Table 1

Comparison of the dielectric measurements of urine phantom at room temperature with data reported in [21]. Dielectric property of the urine phantom measured over 1–4 GHz was used in the frequency domain simulations. The phantom is within 2% of data in [21].

Temperature [°C]	Urine EM property at 915 MHz			Urine EM property at 3 GHz		
	ε_c [21]	ε_c phantom	$\Delta\varepsilon_c$ [%]	ε_c [21]	ε_c phantom	$\Delta\varepsilon_c$ [%]
23	78.4+j42.6	77.7+j42.7	0.7925	74.9+j24.5	74.3+j23.9	1.0767
35	75.2+j52.9	75.5+j53.1	0.3922	72.4+j25.2	71.5+j24.3	1.6603
45	71.6+j60.0	70.3+j59.2	1.6340	69.3+j25.7	68.8+j24.4	1.8845

Table 2

Tissue thermal properties used in the simulations [30,32–34].

Tissue type	Density, ρ [kg/m^3]	Thermal conductivity, k_t [W/m/K]	Blood perfusion rate, ω_b [kg/m^3/s]	Specific heat capacity, C_p [J/kg/K]
Skin	1040	0.32	2.28	3400
Fat	888	0.21	0.50	2387
Muscle	1050	0.56	1.50	3639
Kidney	1060	0.55	17.0	3600
Urine	1000	0.60	-	4200

Specific heat capacity of blood, c_b = 3825 [J/kg/K]

Ambient room temperature, T_r = 20°C

Heat transfer coefficient at T_r, h_a=16 [W/m^2/K]

Table 3

Detector sensitivity of total power radiometer design calculated assuming 500 MHz bandwidth and antenna temperature T_A = 300K for several realistic integration times. Receiver temperature sensitivity is higher for the Dicke radiometer design ($\delta T_D \approx 2\delta T$) [13].

Integration time, τ [s]	Theoretical detector sensitivity for total power radiometer (δT) [K]			
	NF = 0.5 dB	*NF* =1 dB	*NF* = 3 dB	*NF* = 6 dB
1	0.0150	0.0168	0.0265	0.0525
5	0.0067	0.0075	0.0118	0.0235
10	0.0047	0.0053	0.0084	0.0166